Available online at www.sciencedirect.com

jmr&t Journal of Materials Research and Technology

journal homepage: www.elsevier.com/locate/jmrt

Original Article

Experimental characterization of chalcopyrite ball mill grinding processes in batch and continuous flow processing modes to reduce energy consumption

Cesar Celis [a,*], *Antonios Antoniou* [a], *Julio Cuisano* [a], *Adolfo Pillihuaman* [b], *Danmer Maza* [c]

[a] *Mechanical Engineering Section, Pontificia Universidad Católica del Perú, Av. Universitaria 1801, San Miguel, Lima, 32, Lima, Peru*

[b] *Mining Engineering Section, Pontificia Universidad Católica del Perú, Av. Universitaria 1801, San Miguel, Lima, 32, Lima, Peru*

[c] *Laboratory of Microhydrodynamics and Flow in Porous Media, Pontifícia Universidade Católica do Rio de Janeiro, Rua Marquès de São Vicente 225, Rio de Janeiro, RJ, 22451–900, Brazil*

ARTICLE INFO

Article history:
Received 25 August 2021
Accepted 29 October 2021
Available online 10 November 2021

Keywords:
Chalcopyrite
Mineralogy
Rheology
Energy consumption
Batch and continuous ball mill

ABSTRACT

A mineralogy, rheology, and energy consumption-based experimental characterization of chalcopyrite ball mill grinding processes, in both batch and continuous flow processing modes, is carried out in this work. Accordingly, chalcopyrite ore samples are initially characterized in terms of mineralogical composition, particle size distribution, grindability characteristics, and work index. Next, a rheological characterization of actual and lab-created chalcopyrite mineral-slurries is performed. Finally, an energy consumption-based characterization of several chalcopyrite ball mill grinding processes is performed. The results from the initial mineralogical characterization indicate ore samples featuring 5% chalcopyrite. These results also highlight that 80% of the particles present in the chalcopyrite head ore have a diameter smaller than 1386 μm. In addition, they indicate that the Bond ball mill work index is equal to 15.3 kWh/ton, which corresponds to a mineral with the presence of chalcopyrite. The rheological characterization related results indicate that all actual and lab-created mineral-slurries exhibit a shear thinning rheological behavior. These results also show that, because of the higher number of particle interactions, the slurries' apparent viscosity increases with the increase in their solids content. Finally, the energy consumption-based characterization results emphasize that energy consumption is more significantly affected by mill speed than by slurry solids content. Indeed, for the same percentage of mass passing through a 200 mesh, it is found that the specific grinding energy decreases with both the increase in slurry solids concentration and the decrease in mill speed. The results obtained in this work are consistent with findings made in previous studies.

* Corresponding author.
E-mail address: ccelis@pucp.edu.pe (C. Celis).

https://doi.org/10.1016/j.jmrt.2021.10.136

1. Introduction

Mining is a key economic sector worldwide. In Peru, this industry is one of the main drivers for economic growth. This is due to fact that the country has a wealth of mineral resources, including gold, silver, and copper. In mineral processing, the mineral goes through a series of stages before becoming a refined product. The biggest challenge for mineral processing is to both consistently produce high-grade concentrates with maximum recovery of ore deposits [1], and reduce energy consumption in crushing and grinding, which in 1976 was estimated to be about 3.3% of worlds electric energy [2]. When processing minerals, big blocks of raw material called ores are first extracted from mines. Such blocks are next reduced to small fragments subsequently separated between valuable mineral and gangue. Depending on the mineral type and the size of the ore extracted from a mine, the ore size reduction phase involves crushing and grinding stages. Crushing is the process where the ore coming directly from a mine is reduced to smaller sizes. Usually crushing by itself is not enough to release the valuable mineral because the obtained ore fragments need an even larger size reduction [1]. In grinding processes, therefore, there is a further size reduction of ores coming from the crushing stage. Ore grinding, commonly employed in the processing of metallic minerals, requires a large capital investment, and it is often the area of maximum use of power and wear-resistant materials in a concentrator plant [3].

Ore grinding can be dry or wet. Nevertheless, compared to the dry case, wet grinding presents several advantages, including lower operating temperature, dust and fragment resistance, and better handling features in mineral volumetric classification. Because of the large amounts of energy consumed in ore grinding processes [4], there is always a need to study options to reduce the referred energy consumption, and to improve ore grinding energy efficiency [5]. It is worth noticing that significant heat is usually generated in ore grinding, and this can be considered as an efficiency related loss. Heat is however an inevitable consequence of material breakage [6]. In practice, several parameters affect the performance of ore grinding processes. Accordingly, using a laboratory scale ball mill, the influence on energy efficiency of some of these parameters, including charged material volume, ball filling ratio, and mill rotational speed, was experimentally studied by Sabah et al. [7]. Similarly, Ouattara and Frances [8] analyzed, in terms of particle size distribution, suspensions rheological behavior, and grinding efficiency, the influence of different operational parameters on calcite suspensions grinding performance. It was found that the specific energy input leading to a required product quality varies.

In previous studies [8–11], stirred media milling has been shown to produce ultrafine particles from coarser ones. In such mills, material fragmentation comes from both compression and shear induced by high-speed rotating grinding beads including impellers (agitators). Factors affecting both wet grinding and dispersion in stirred media mills relate to (i) grinding chamber and stirrer geometries, (ii) operating parameters (grinding time, stirrer speed, bead filling ratio, bead size), (iii) mill operation mode (continuous, batch, pendular, circulating), and (iv) suspension features (solid concentration, particle size, additives). A stirred media mill was used in [12] to monitor on-line the rheological characteristics of the associated suspension and their influence on grinding processes. It was particularly observed that the suspension rheological behavior strongly affects the grinding performance, in terms of particle specific surface area, size distribution, and specific grinding energy. It is known that stirred media mills have better energy efficiency than ball ones in fine and ultra-fine grinding processes. So past works [13] have been focused on determining whether or not this better performance of stirred mills, over ball ones in fine grinding, can be also extended to coarse grinding applications. From such assessments, it has been found that, for laboratory scale mills, up to 30% energy saving can be obtained by using stirred mills instead of ball ones.

Vertical roller mills, combining in single units crushing, grinding, classification, and drying processes, and leading to energy savings when compared to conventional ball milling, are usually employed to comminute cement raw materials. To assess the feasibility of extending this vertical mills' improved performance to ore grinding applications, Altun et al. [14] studied chalcopyrite ore grinding processes using a vertical roller mill-based pilot plant. The results indicate that by doing

Nomenclature

Variables

Cw	Solids weight (mass) concentration
d	Diameter (particle)
$F_{critical}$	Upper-tail percentage point of F distribution
$F(x)$	Percentage of mass passing
F_x	x% passing particle size (head ore)
F_0	Test statistic or F ratio for null hypothesis
G_{bp}	Grindability index
k	Model parameter
m	Model parameter
P_i	Mesh opening
P_x	x% passing particle size (product)
W_i	Bond work index
x	Mesh opening
$\dot{\gamma}$	Shear rate
η	Apparent viscosity
η_0	Apparent viscosity at zero shear rate
η_∞	Apparent viscosity at infinite shear rate
λ	Fluid relaxation time

Abbreviations

ANOVA	Analysis of variance
cp	Chalcopyrite
C–Y	Carreau-Yasuda
F	Feed
GG	Gangue
GGS	Gates-Gaudin-Schuhmann
ICDD	International center for diffraction data
mt	Magnetite
PSD	Particle size distribution
XRD	X-ray diffraction

so up to 18% savings in specific energy consumption and less wear on internal components can be obtained. In a similar study [15], it was concluded that the specific grinding energy consumption has a direct correlation with both product size and mass flow rate. Conventional ore grinding is typically carried out using tumbling mills, i.e., rod and ball mills. Rod-based mills are generally used for relatively coarse grinding, whereas ball ones are employed when finer particles are required. In this sense, an energy-based ball mill model suitable to applications ranging from batch to continuous operation mode grinding is proposed by Shi and Xie [16]. The developed model allows simulating the effect of changing ore breakage characteristics on ground product size distribution. Finally, notice that batch grinding processes are employed as well to study grinding performance in terms of particles size distribution and specific surface area [17].

The main focus here is on ore grinding and its associated energy consumption. As such, this work describes a mineralogy, rheology, and energy consumption-based experimental characterization of chalcopyrite ball mill grinding processes, carried out in both batch and continuous flow processing modes. In terms of contributions to knowledge, the rheological characterization of actual and laboratory mineral-slurries, carried out by measuring their apparent viscosity as a function of flow shear rate, constitutes one of the original contributions of this work. Other contributions relate to both the mineralogical characterization of chalcopyrite samples and the energy consumption measured in the several ball mill grinding processes performed using a pilot plant. Accordingly, after this introduction, Sections 2 and 3 describe, respectively, the chalcopyrite mineralogical and rheological characterizations carried out in this work. The energy consumption characterizing several chalcopyrite ball mill grinding processes, performed in both batch and continuous flow processing modes, are discussed in Section 4. Finally, Section 5 summarizes the main conclusions drawn from the results obtained here.

2. Chalcopyrite mineralogical characterization

The chalcopyrite mineralogical characterization carried out here is described in this section. In addition, a first study of batch grinding processes focused on assessing particle size distribution, grindability characteristics, and work index is also discussed. The results obtained from this first study were used as ingredients to define the parameters characterizing the mineral slurries studied in both rheological (Section 3) and energy consumption (Section 4) based terms.

2.1. Materials and methods

2.1.1. Samples preparation (sampling, sizing and quartering)

The chalcopyrite studied in this work was obtained from a Peruvian mining company [18] focused on the production of copper concentrate. The head ore was delivered in five (5) bags of about 1 ton each (Fig. 1, left), featuring particle sizes of about ¼ inch or less. For the mineralogical characterization carried out here, about 100 kg of mineral, at particle sizes of 2 mm or less (10 mesh), 100% of the sample, were required. Therefore, due to the characteristics of the chalcopyrite head ore and the total amount available, to obtain the ore samples to be analyzed, the quartering method was utilized.

Accordingly, with the help of a shovel, following the incremental sampling technique, several samples from a bag were first extracted. This technique consists of taking samples from twelve (12) zones (blue dots in Fig. 1, center) located at four (4) cardinal points on each of the bag concentric radii utilized, three (3) in this work. This bag ore extraction process was carried out in a continuous and homogeneous manner until the required 100 kg of chalcopyrite were accumulated. After obtaining the representative 100 kg ore sample, next, using a roller crusher (Fig. 1, right) and a high-capacity sieve, the ore size was reduced from ¼ inch to particle diameters of about 2 mm. The ground sample thus obtained was finally quartered (in successive halves) using a Jones riffle splitter, until obtaining samples of 1 kg each. These final samples were weighed, bagged, and left ready for the mineralogical characterization tests performed.

2.1.2. Mineralogical characterization

The mineralogical analyses were carried out on a representative sample of chalcopyrite fines, which were obtained by grinding the quartered samples discussed in Section 2.1.1. The associated mineralogical characterization was performed using both X-ray diffraction (XRD) and optical microscopy

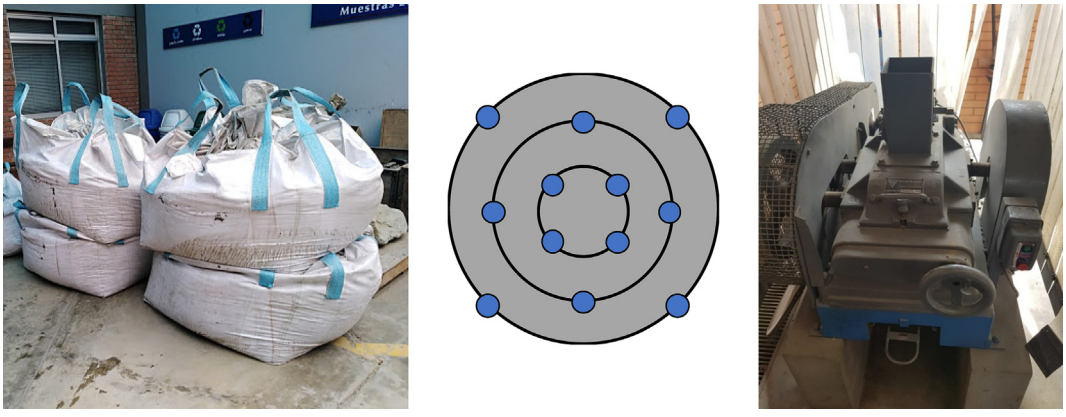

Fig. 1 – Chalcopyrite head ore (left), bag sample points (center) and roller crusher (right).

Table 1 – Standard meshes used in the granulometric characterization.

Mesh	16	18	25	35	45	60	80	120	170	200
Opening [μm]	1180	1000	710	500	355	250	180	125	90	75

techniques [19]. Notice that XRD allows semi-quantitatively determining the samples crystalline phases. More specifically, phase identification was performed based on the ICDD (International center for diffraction data) database, whereas phase quantification was do so by using the Rietveld refinement method. In the mineralogical analyses by optical microscopy, the estimated percentages of free and intergrown grains were determined. In addition, the mineral species present in the samples were identified, and the textures of their intergrowths were characterized.

2.1.3. *Granulometric characterization*

The particle size distribution (PSD) characterizing the chalcopyrite head ore was determined using the standard meshes method. As shown in Table 1, this method involves gradually sieving the sample on 10 different meshes. At each sieving, the mass of ore retained on each mesh is weighed, which is used then to calculate the corresponding mass percentage. Samples with particles smaller than 75 μm (200 mesh) are considered as surplus. Results of particle size analyses are usually generalized using size distribution functions, which relate particles size (sieve opening retaining or allowing particles to pass) to percentage mass (weight), cumulative or passing. In practice, to represent particle size distributions, the Gates-Gaudin-Schuhmann (GGS) distribution function,

$$F(x) = 100\left(\frac{x}{k}\right)^{m}, \quad (1)$$

is usually employed. In this equation, $F(x)$ represents the percentage mass passing, x the mesh opening (μm), and the constant parameters k and m are obtained from the linearized form of Eq. (1). In this work, to determine the F_{80}, i.e., the mesh opening diameter through which 80% (by mass) of particles pass, an extrapolation process of the experimentally determined particle size distribution (GGS function) is carried out.

2.1.4. *Grindability and work index*

Grindability studies allow determining, as a function of both grinding time and work input, the particle size distribution of the processed ore. Two grindability related sets of assessments have been initially carried out in this work. The first one was focused on determining, for each mesh size, the grindability curves (as a function of grinding time) characterizing the chalcopyrite ore studied in this work. Following existing literature [20], thus, a batch ball mill (Fig. 2, left) featuring a mass ratio of ore to water equal to 2, i.e., 1000 g of ore per 500 g of water, was employed in the first set of assessments. In addition, chalcopyrite grinding processes for six (6) different grinding times, 5, 10, 15, 20, 25, and 30 min, were performed. For a given grinding time, then, after milling the chalcopyrite ore, the sample was sieved through a 200 mesh, and the non-passing ore was dried in an oven until removing all its water content. Using the meshes highlighted in Table 1, a granulometric analysis of the dry sample was finally performed. This procedure was repeated for each grinding time accounted for.

The second set of assessments focused on determining the Bond ball mill work index characterizing the chalcopyrite ore analyzed here. Accordingly, a standard Bond ball mill (Fig. 2, center) was employed for this purpose. Notice that the Bond work index is an energy consumption related parameter, which indicates the energy needed to reduce ore sizes so that 80% (in mass) of a sample passes through a 75 μm mesh opening ($P_{80} = 75\ \mu m$) [21]. As it may be expected, this index is directly related to the specific ore used in the grinding processes. When determining the work index, the initial head ore features particle sizes smaller than 3.35 mm and a bulk volume of 700 cm^3. Shortly [21], a Bond test involves a dry closed loop one with sieving of the mill product after each stage, fines replaced by equal amounts of fresh feed material, and variation of grinding times to achieve material recirculating loads

Fig. 2 – Batch ball mill (left), standard Bond ball mill (center), and Bond procedure (right).

of 250%. This Bond procedure is schematically highlighted in Fig. 2 (right).

The grinding cycles described above are carried out successively until the last three results are similar with an error margin of ±20 g. Finally, with the obtained results, the Bond ball mill work index (W_i) is computed from [21],

$$W_i = \frac{44.5}{P_i^{0.23} \cdot G_{bp}^{0.82} \cdot \left(\frac{10}{\sqrt{P_{80}}} - \frac{10}{\sqrt{F_{80}}}\right)}, \quad (2)$$

where P_i represents the mesh opening (μm), G_{bp} the grindability index (average of the last 3 cycles), and F_{80} and P_{80} are, respectively, the 80% passing particle sizes (μm) associated with the mill feed (head) and the final product (last cycle). Bond [21] also proposes using correction factors applicable to cases involving open circuit grinding, too coarse feeds, fines excessive overgrinding, and low size reduction ratios in mills. He points out that in those cases where the P_{80} value cannot be determined experimentally, as an approximation, average values can be adopted. For instance, for a 200 mesh (75 μm mesh opening), a $P_{80} = 50\ \mu m$ can be employed.

2.2. Results and discussions

The main results obtained from both the mineralogical characterization and the first batch grinding processes carried out are summarized here.

2.2.1. Mineralogical characterization

As shown in Fig. 3 (left), the mineralogical analysis of the chalcopyrite head ore shows that, in terms of overall mineralogical composition, this ore is formed by chalcopyrite (5%), magnetite (15%), mineral gangues (78%), and traces (<0.5%) of sphalerite, pyrite, digenite, covellite, and goethite. It has been also found that chalcopyrite and magnetite are almost entirely associated among them and with other mineralogical species. The presence of pyrite is relatively scarce, being observed as inclusions in gangues and in direct contact with chalcopyrite. In addition, Fig. 3 (center and right) shows two photomicrographs, one at a sample magnification of 400 μm (center) and the other at 50 μm (right), representative of the mineralogical analysis carried out. From Fig. 3 (right), in particular, it is noticed fragments composed of gangues (GGs) in lateral association with chalcopyrite (cp) and magnetite (mt).

2.2.2. Granulometric characterization

The chalcopyrite head ore particle size analysis, performed using the standard meshes method, allowed determining the associated particle size distribution. The results from the referred analysis are summarized in Fig. 4. More specifically, Fig. 4 (left) shows both the experimental results obtained in this work and the GGS distribution function curve-fitted on these results. The constant parameters k and m appearing in Eq. (1) have been obtained, in turn, from the straight line curve-fitted to the log–log plot (Fig. 4, right) constructed using the original experimental data. The GGS distribution function so determined allowed obtaining, through an extrapolation process, the F_{80} characterizing the chalcopyrite sample accounted for. F_{80} in this work is equal to 1386 μm, which means that 80% of the particles present in the chalcopyrite head ore have a diameter smaller than 1386 μm.

2.2.3. Grindability and work index

The grindability tests carried out here allowed determining the product particle size distribution as a function of both grinding time and work input. Accordingly, the grindability curves associated with the chalcopyrite ore studied in this work, for each mesh size as a function of grinding time, are illustrated in Fig. 5. Notice that, in all tests performed in this work, the 200 mesh (75 μm opening) was chosen as the passing mesh parameter. It is particularly noticed from Fig. 5 that, as it may be expected, for a given mesh size, the percentage mass passing increases with the increase in grinding time. Similarly, for a given grinding time, the percentage mass passing increases as well with the increase in mesh opening (reduction in mesh number). This last aspect is particularly true for relatively low grinding times.

In addition, Table 2 summarizes the main experimental results obtained from the several grinding processes carried out using a standard Bond ball mill. Results from this table have been used to compute the Bond ball mill work index characterizing the chalcopyrite ore analyzed in this work. More specifically, accounting for a $P_{80} = 50\ \mu m$ (Section 2.1.4), F_{80} equal to 1386 μm (Fig. 4), G_{bp} of 1.0874 g per revolution (Table 2 last cycle), and a (200) mesh opening of 75 μm, the calculated work index is equal to 15.3 kWh/ton, which corresponds to a mineral with presence of chalcopyrite. Finally, notice that the results discussed in this Section 2 have been used to define the mineral slurries studied in the following sections.

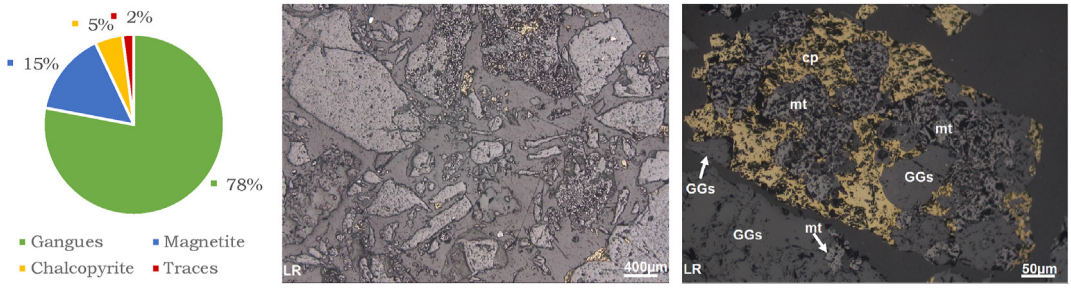

Fig. 3 – Ore mineralogical composition (left) and photomicrographs at sample magnifications of 400 μm (center) and 50 μm (right).

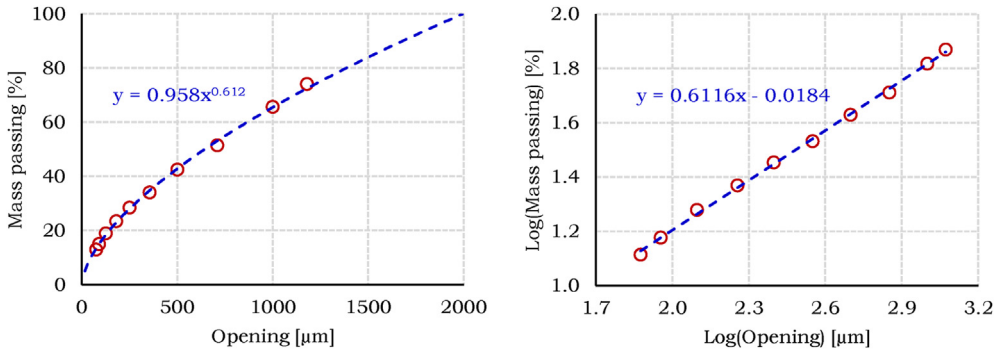

Fig. 4 – Chalcopyrite ore particle size related results in both linear (left) and log–log (right) scales.

3. Chalcopyrite slurries rheological characterization

In this section, the chalcopyrite rheological characterization carried out in this work is discussed. A particular emphasis is put on the mineral-slurries studied here and the actual rheological measurements performed.

3.1. *Materials and methods*

3.1.1. *Mineral-slurries*

Mineral processing often involves transporting and grinding mixtures of water and/or chemical solutions, carrying crushed or ground minerals, known as mineral-slurries [22]. Mineral-slurries are indeed mixtures of a carrying fluid (water and/or chemical solutions) and suspended solids (ground rocks). To properly describe mineral-slurry related processes, many factors, including particles size distribution and slurry viscosity, need to be accounted for [23]. Based on their rheological behavior, mineral-slurries may exhibit Newtonian or non-Newtonian rheological properties [24]. Consequently, to properly operate mineral-slurry based systems, the associated complex flows need to be carefully characterized.

Accordingly, two sets of mineral-slurry samples have been rheologically characterized in this work. First, actual mineral-slurry samples, extracted from a ball mill discharge section of a copper concentrator plant [18] operating with the same chalcopyrite head ore studied here, were initially analyzed. The actual mineral-slurry samples showed a solids weight (mass) concentration (Cw) of 66%. Second, in order to analyze the effect of solids content on the mineral-slurries rheology, four additional slurries featuring different solids weight concentrations (50, 60, 66, and 70%) were also examined. These additional mineral-slurries were artificially created in a lab using the chalcopyrite head ore discussed in Section 2. More specifically, the chalcopyrite ore was crushed to sizes under 3.36 mm (mesh 6) before grinding it. Next, to obtain the four slurries, two grinding process, at 50 and 66% of solids weight concentration in water, were conducted in a lab-scale ball mill. The product resulting from the grinding process at 66% was dried and rehydrated with deionized water to produce slurries at 50, 60, 66, and 70% solids concentrations. These drying and rehydration processes were carried out to increase

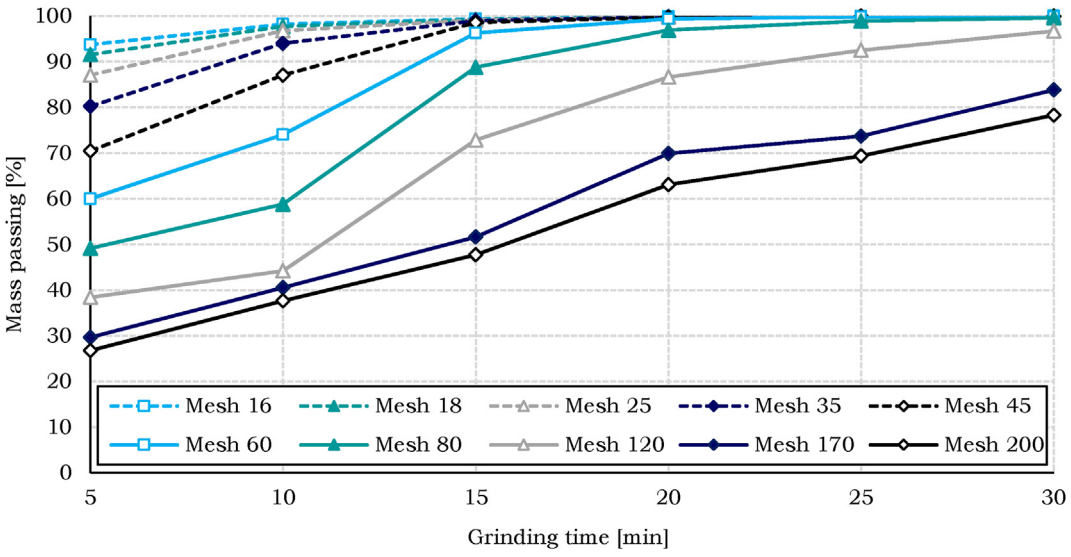

Fig. 5 – Chalcopyrite head ore grindability.

Table 2 – Standard Bond ball mill results.

Cycle	Number of revolutions	Total fines [g]	Produced fines [g]	Grindability index (G_{bp})	Fines to be produced [g]	Number of revolutions for next cycle
1	100	315.3	85.1	0.8511	465.1	546
2	546	546.5	505.5	0.9251	392.8	425
3	425	500.5	429.5	1.0105	397.9	394
4	394	489.7	424.7	1.0778	399.1	370
5	370	442.3	378.7	1.0234	404.3	395
6	395	486.2	428.7	1.0853	399.5	368
7	368	450.3	387.1	1.0519	403.4	383
8	383	431.3	372.8	0.9733	405.5	417
9	417	509.4	453.4	1.0874	396.9	365

the number of mineral-slurry samples to be analyzed. Notice that the use of deionized water reduces the liquid phase pH or ionic effects on the mineral-slurries rheological behavior. Finally, to verify the methodology followed here, the rheological characteristics of the mineral-slurry coming from the grinding process at 50% were compared with the corresponding ones characterizing the slurry ground at 66% and rehydrated at 50%.

3.1.2. *Granulometric characterization*

In a similar fashion to what is described in Section 2.1.3, the particle size distributions characterizing the mineral-slurries analyzed here were determined using the standard meshes method. As highlighted before, this method involves gradually sieving samples on ten (10) different meshes (Table 1). In addition, at each sieving, the mass of ore retained on each mesh is weighed and used to compute the corresponding mass percentage. Samples with particles smaller than 75 μm (200 mesh) are considered in this case as surplus.

3.1.3. *Rheological characterization*

The rheological characterization was carried out using a Discovery HR-3 rotational rheometer [25]. This rheometer features a concentric cylinder Couette geometry including both a stationary outer cylinder (cup) and a rotating inner (bob or rotor) one (rotor height = 42 mm, rotor diameter = 28 mm, gap = 2 mm). This geometry is suitable to characterize suspensions because the gap between the rheometer cup and the rotor helps to reduce the probability of particle settlement during a test [26,27]. Notice that two main particles related phenomena take place during rheological tests, particle interactions and particle settlement. For a constant shear rate, particle interactions produce a constant stress response, but, from the onset of settlement, the shear stress becomes time dependent [28]. This is why in this work the rheological measurements were carried out at constant shear rates, accounting for a specified time period of 60 s. In this way, it is possible to both infer when gravity effects show up and select data coming exclusively from particle interactions.

In this work, 08 different shear rates, ranging from 10 to 500 s^{-1}, were assessed. This shear rate range represents most processes found in industrial applications and slurries transport [29]. All measurements were made at 24 °C, a temperature commonly found in mineral-slurries processing [28]. This temperature was controlled with both a rheometer embedded Peltier cell and a fluid thermal controller Thermo CUBE. To reduce the uncertainties associated with the rheological measurements, each test was repeated three times. As such, two types of uncertainties were accounted for, random and systematic. The first one was defined as the standard deviation of the three measured viscosity values. The systematic uncertainty was defined, in turn, as the uncertainty specific to the measurement system. Thus, it was estimated from the mean of the standard deviations of each measurement.

3.2. *Results and discussions*

The main results obtained from the rheological characterization of both actual and lab ground mineral-slurries carried out are discussed in this section.

3.2.1. *Particles size distribution*

The particle size distributions (PSD) characterizing the mineral-slurries analyzed in this work are shown in Fig. 6. This figure also includes the Gates-Gaudin-Schuhmann (GGS) distribution functions (Eq. (1)) curve-fitted to the experimental values obtained here. In turn, the constant parameters k and m associated with these GGS functions are summarized in Table 3. From the results shown in Fig. 6 (left), it is possible to see that the actual mineral-slurry (mine grinding), coming from the discharge section of a concentrator plant ball mill, features coarser particles (Table 3) than the laboratory slurry ground at the same solids concentration. Some of these discrepancies come from the different mill rotation velocities, grinding systems scales, and mill ball distributions characterizing these grinding processes. The influence of these parameters on the slurries' rheological behavior will be discussed in Sections 3.2.2 and 3.2.3.

Figure 6 (right) also shows that the lab-ground mineral-slurry at 66% solids concentration features finer particles than the one at 50%. This result is somehow expected because, at higher solids concentrations, the probability of collision between balls and mineral particles is higher, then the produced particles are finer. This last aspect is also highlighted by the characteristic particle diameters shown in Table 3. Notice that d_{50} (d_{80}) indicates that 50% (80%) of the particles present in a mineral-slurry have a diameter (in μm) smaller than the value included in this table for the referred slurry.

3.2.2. *Effects of solids weight concentration on rheology*

As highlighted in Section 3.1.1, as a means of verification of the methodology followed here, the rheological characteristics

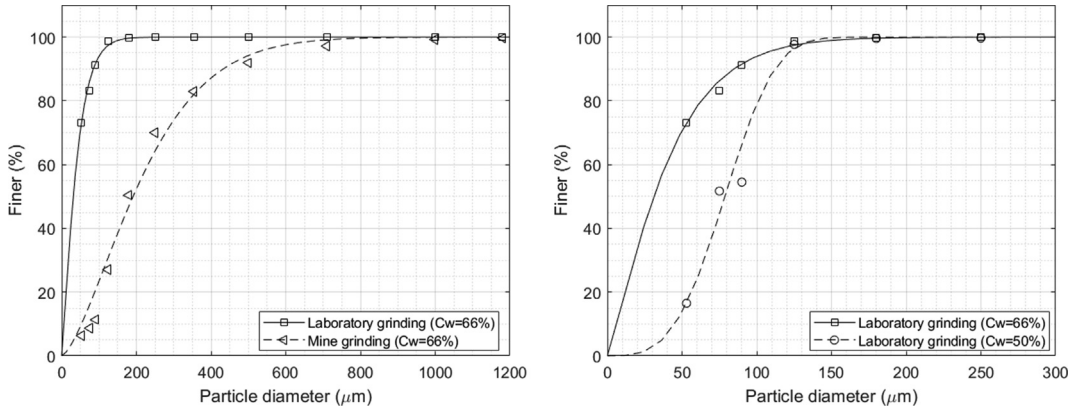

Fig. 6 – PSD characterizing both actual and lab mineral-slurries. Symbols: actual measurements. Continue and dashed lines: Gates-Gaudin-Schuhmann (GGS) distribution function.

Table 3 – GGS function parameters and characteristic particle diameters.

	k	m	d_{50} [μm]	d_{80} [μm]
Actual mineral-slurry 66%	8.0961	1.4717	191.2	338.9
Lab mineral-slurry 66%	4.4833	1.1984	31.0	62.7
Lab mineral-slurry 50%	15.257	3.4109	78.7	100.7

of the lab-created mineral-slurry coming from a grinding process at 50% solids weight (mass) concentration have been compared to the corresponding ones characterizing the slurry ground at 66% and rehydrated at 50%. The results from the referred comparison are highlighted in Fig. 7 (left). As noticed from this figure, both artificially created slurries feature similar rheological characteristics. Indeed, the apparent viscosity related curves follow the same trends, and their associated values are of the same order of magnitude (average discrepancies ~10%). This outcome emphasizes that, for a particular grinding system, a mineral-slurry ground at a given solids concentration (66%), and diluted at a different one (50%), leads to a viscosity-related curve that is similar to the one that would have been obtained if this slurry had been originally ground at the concentration used for dilution purposes (50%). From Fig. 7 (left), it is worth noticing as well that the mineral-slurry ground at 66% (d_{50} = 31.0 μm, Table 3) exhibits a lower viscosity than the one ground at 50% (d_{50} = 78.7 μm, Table 3). This result may be expected because the slurry ground at 66% features a finer PSD (Fig. 6, right), and both particle interactions and slurry viscosities are directly proportional to the square of the particles size [30,31].

In addition, the rheological characteristics of the mineral-slurry ground at 66%, dried and rehydrated at 50, 60, 66, and 70% solids concentration, are shown in Fig. 7 (right). From this figure, it is possible to observe that the measured apparent viscosity decreases with the increase in the shear rate. This means that the studied mineral-slurries can be characterized as non-Newtonian fluids belonging to the shear thinning or pseudoplastic category. Besides, Fig. 7 (right) also shows that the slurry viscosity increases with the increase in the slurry solids content. This last outcome can be attributed to the fact that the interaction between particles increases with the increment in solids concentration [32]. It is worth noticing as well that, at relatively low solids concentrations (50 and 60%) and high shear rates (>10^2 s^{-1}), the measured viscosities tend to increase with the increase in shear rate. This rheological behavior clearly disagrees with the expected monotonic shear thinning one. It is important to highlight here that this outcome is related to the secondary flows arising during the

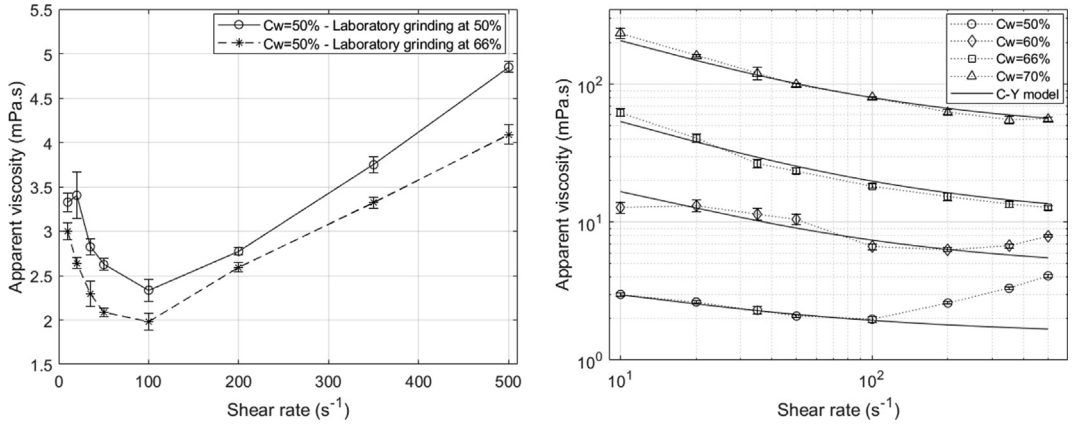

Fig. 7 – Influence of solids weight concentration on lab mineral-slurries rheology. Symbols: actual measurements. Vertical bars: measurement uncertainties.

experiments. These flow patterns appear when the fluid layers that move uniformly between the rheometer cup and rotor lose their stability, developing internal rotations, and leading to both a random distribution of particles and an increase in shear stresses, which increases in turn viscosity [33,34]. Therefore, these specific viscosity measurements carried out during the referred flow instabilities do not reflect the fluid rheological behavior and they need to be disregarded.

The experimental results shown in Fig. 7 (right) have been also curve-fitted using the theoretical non-Newtonian model Carreau-Yasuda (C–Y). Notice that this model is well suited to represent the rheological behavior of pseudoplastic fluids as they are bi-viscous (two viscosity levels) ones [35]. In the C–Y model, the apparent viscosity (η) is estimated from,

$$\frac{\eta-\eta_{\infty}}{\eta_0-\eta_{\infty}}=\left[1+(\lambda\dot{\gamma})^2\right]^{\frac{n-1}{2}}, \tag{3}$$

where η_0 and η_{∞} represent the viscosity thresholds at zero (0) and infinite (∞) shear rates, respectively. λ is in turn the fluid relaxation time, $\dot{\gamma}$ the shear rate, and n the power index. These model parameters, derived from the experimental data characterizing the lab mineral-slurries analyzed here, are summarized in Table 4. Notice that these model parameters, which change with the slurries' solids concentration, are useful in the numerical modeling of mineral-slurry transport and grinding processes.

3.2.3. *Effects of ore composition and grinding system on rheology*

Regarding ore composition first, overall, the experimental results obtained in this work concur with past efforts focused on rheological characterization of mineral-slurries (Fig. 8, top). For instance, the works by Zhang and Peng [27] and Sun et al. [36] involve ores with mineralogical compositions similar to the one characterizing the ores studied here. Accordingly, for similar solids concentrations, the apparent viscosities measured previously and in this work are of the same order of magnitude. Compared to the present work, however, for solids concentrations less than 50%, the works by Bhattacharya et al. [29] and Singh et al. [37], which involved lateritic nickel and iron based slurries, respectively, present higher levels of viscosity. This means that mineral-slurries' rheological behavior is also strongly dependent on ores' mineralogical composition. This is somehow an expected result because each ore involves specific grinding requirements, so after grinding them it is expected that the resulting slurries also feature different rheological characteristics. Notice as well that all slurries accounted for in the referred studies exhibit a shear thinning behavior, which supports the results of the present work.

Second, as shown in Fig. 8 (bottom), the actual mineral-slurry coming from the discharge section of a concentrator plant ball mill (mine grinding) also exhibits a shear thinning behavior. From this figure, it is also possible to see that the actual mineral-slurry follows the same viscosity trend as the lab created one, but their viscosity values are slightly shifted upwards. These slightly higher viscosities observed for the same solids concentration are related to the grinding system employed to produce the mineral-slurries studied here. The actual mineral-slurry features indeed more coarse particles than the lab created one (Fig. 6, left). Notice that coarser particles have more inertia so their acceleration/deceleration during particle migration and interaction requires more energy, resulting in an increase in apparent viscosity [32]. This effect may be partially responsible for the results shown in Fig. 8 (bottom).

Summarizing, at the solids content analyzed, all actual and lab ground mineral-slurries studied here exhibit a shear thinning rheological behavior. The actual mineral-slurry features viscosity levels slightly higher than those associated with the lab created one. The results also show that, because of the larger number of particle interactions, the slurries' apparent viscosity increases with the increase in their solids concentration. In addition, when compared to other results available in previous works, the experimental ones obtained here present reasonably agreement, which supports the findings discussed in this work. Finally, from the experimental data obtained in this work, material coefficients associated with the non-Newtonian Carreau-Yasuda model were determined. These coefficients will be helpful in the numerical modeling of transport and grinding processes involving the mineral-slurries accounted for here.

Table 4 – Carreau-Yasuda model material coeficientes.

Parameter	50%	60%	66%	70%
η_0	3.8	25	105	400
η_{∞}	1.5	4.5	10.5	45
λ	0.2	0.2	0.3	0.3
n	0.45	0.35	0.32	0.32

4. Energy consumption-based characterization

The energy consumption-based characterization of different chalcopyrite grinding processes, performed in ball mills using both batch and continuous flow processing modes, is discussed in this section.

4.1. *Materials and methods*

4.1.1. *Chalcopyrite mineral samples*

The chalcopyrite grinding processes, in both batch and continuous modes, were carried out using a 200 kg sample of chalcopyrite head ore, extracted according to the methodology described in Section 2.1.1. More specifically, following the incremental sampling technique, several samples were first extracted from a bag until obtaining the required 200 kg of chalcopyrite. After doing so, next, using a roller crusher (Fig. 1, right) and a high-capacity sieve, the ore size was reduced to particle diameters of 2 mm or smaller. Finally, using a Jones riffle splitter, the chalcopyrite sample was quartered in successive halves. About 50 kg of the chalcopyrite sample were used in the batch mode grinding tests, and the remaining 150 kg in the continuous mode ones (pilot plant).

4.1.2. *Granulometric characterization*

Following the methodology described in Sections 2.1.3 and 3.1.2, and using the standard meshes method, the particle

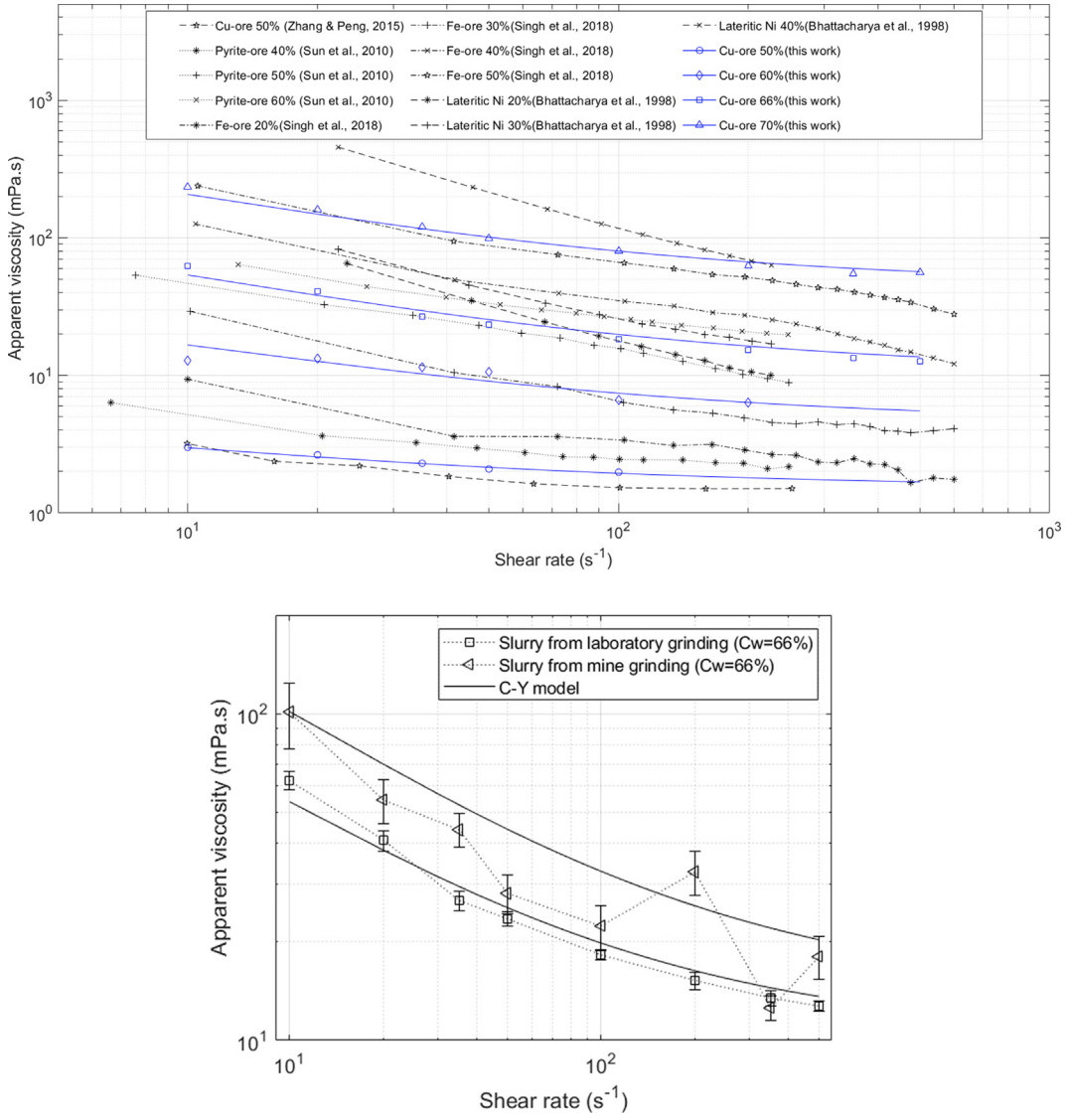

Fig. 8 – Mineral-slurries rheology from previous and present works. Vertical bars: measurement uncertainties.

size distributions characterizing the mineral-slurries obtained from ball mill grinding processes performed were determined. As emphasized above, this method involves gradually sieving ore samples on 10 different meshes (Table 1), so the mass of ore retained on each sieving mesh is weighed and used to compute the corresponding mass percentage. Samples with particles smaller than 75 μm (200 mesh) are considered as surplus.

4.1.3. *Chalcopyrite grinding in batch processing mode*

In each batch milling test carried out, in mass terms, an amount of chalcopyrite ore equal to 1 kg was utilized. The parameters studied were both the solids concentration (content) in the slurry and the mill speed. These variables were chosen because of their influence on both the particle size distribution and the associated energy (power) consumption. According to previous works, recommended values for the first parameter (slurry solids) are in the range between 65 and 80% [38]. For the second parameter (mill speed), in turn, suggested values are around 75% of the mill critical speed (108.3 rpm, in this case) [39]. Accordingly, three different contents of solids in the mineral-slurry (56, 66, and 76%) and three mill (rotational) speeds (56, 70, and 84 rpm) were studied in this work. Therefore, accounting for a full factorial design and considering two replicates for each test, a total of 18 batch milling tests, each lasting 40 min, were carried out. The order of these milling tests was randomly defined according to the full factorial design of experiments matrix described in Table 5. All chalcopyrite grinding processes performed in batch mode were carried out employing a 0.5 hp ball mill. Some of the parameters measured during the experimental tests (under the IEC/EN 61000-4-30, class A, standard) include voltage, current, power, and power factor.

Since all chalcopyrite ore samples milled in batch initially featured a mass of 1 kg, the amount of water to be added to the ball mill, as a function of the required solids content in the slurry, was first determined. Consequently, each batch milling test was started by introducing into the mill both the mineral

Table 5 – Experimental matrix for the batch tests according to the full factorial design.

Run	Replicate	Mill speed [rpm]	Slurry solids [%]	Run	Replicate	Mill speed [rpm]	Slurry solids [%]
1	2	84	66	10	1	70	76
2	1	84	66	11	2	56	76
3	1	56	66	12	2	70	76
4	2	70	56	13	1	56	76
5	1	70	56	14	1	70	66
6	2	84	76	15	2	70	66
7	1	84	56	16	2	84	56
8	2	56	56	17	1	56	56
9	1	84	76	18	2	56	66

and the required water. At this point, the frequency inverter employed in the tests was set to allow the mill rotating at the desired speed, and the network analyzer began the data acquisition. The mill speed was then checked using a contact photoelectric type tachometer and the milling time was counted. After completing a batch grinding process, the ball mill was turned off and the mineral slurry was extracted from inside the mill. The removal of the mineral-slurry was carried out with the help of water, so that no mineral remained inside the mill and did not affect the next test, nor the result of the test in progress. Next, using the smallest mesh size employed in the particle size analysis (200 mesh) (Table 1), the mineral slurry was sieved. Notice that the slurry that passed through this mesh, including the fines present in it, was discarded. This process was carried out to reduce the mineral-slurry humidity and facilitate the drying of the remaining mineral. To obtain the particle size distribution, once the dry sample was obtained, its corresponding granulometric analysis was carried out.

4.1.4. *Chalcopyrite grinding in continuous processing mode*

Previous works [1,40] highlight that slurry solids content, mill speed, and slurry viscosity are some of the factors that directly affect mill grinding efficiency. Following these works, then, using a laboratory scale pilot plant, the solids concentration (content) in chalcopyrite mineral-slurries has been studied in this work. More specifically, the influence of this parameter on the associated particle size distribution and energy (power) consumption has been analyzed. Accordingly, three different contents of solids in mineral-slurries (66, 70, and 75%) have been studied here. Accounting for a full factorial design then, and considering two replicates for each test, a total of 6 continuous milling tests, each lasting 60 min, have been performed. In a similar fashion to the batch cases, the order of the continuous milling tests was randomly defined according to a full factorial design of experiments matrix. It is worth noticing that, in all continuous mode grinding tests performed, the ball mill rotation speed was kept constant and equal to 54 rpm. In addition, the chalcopyrite ore feed rate was equal to 25.55 kg/h. Finally, for the slurries featuring 66, 70, and 75% solids, the water feed rate was equal to 16.5, 12.8 and 8.5 kg/h, respectively.

All continuous flow grinding tests were performed in a laboratory scale pilot plant, which operates in closed loop and includes a mineral feed hopper, a continuous-type ball mill, a slurry centrifugal pump, and a helical classifier. Briefly, in this pilot plant, the chalcopyrite ore is fed through the hopper and dosed by a vibrating feeder. At the same time, regulated by a globe valve and measured by a Coriolis-type mass flow meter, water enters the continuous milling system through pipes and hoses. The chalcopyrite ore is ground inside the mill by steel balls and the slurry discharge takes place at the end opposite to the feed. After discharge, the slurry is directed to the helical classifier. In this last device, the ore is classified into fine and coarse particles. The fine product is discharged from the classifier bottom, whereas the coarse one is discharged from the top, allowing it to be recirculated back to the ball mill for regrinding. Finally, it is worth noticing that, during all continuous mode grinding tests carried out in the referred pilot plant, power consumption and mass flow rates were continuously measured. Also, at grinding times 5, 10, 15, 20, 30, 40, 50, and 60 min of each milling test, chalcopyrite slurry samples were extracted for their corresponding analyses. These samples were weighed (mineral-slurry weight) on an electronic balance, labeled, and placed in a lab-scale electric oven to be dried and then analyzed. Next, after evaporating the water in the samples, the remaining masses were weighed (dry mineral weight) and particle size analyses were performed using the standard mesh method (Section, 2.1.3, Table 1).

4.1.5. *Analysis of variance*

Due to different variability sources, the measurements carried out in both batch and continuous grinding processes featured some spread or variability. Therefore, a statistical analysis was performed to determine whether the levels of the studied factors (slurry solids and mill speed) affect the parameters of interest (product particles size and energy consumption), or the changes in these parameters come from the factors observed variability. The referred statistical analysis carried out based on one of the most widely employed techniques in the field of statistical inference, analysis of variance (ANOVA) [41]. More specifically, for the batch milling tests, a two-factor (slurry solids and mill speed) analysis featuring 3 levels per factor and 2 test replicates was accounted for. For the case of the continuous milling tests, in turn, a single-factor (slurry solids) analysis with 3 levels and 2 test replicates was considered. Accordingly, following a classical analysis of variance approach [41], for the hypothesis of no differences in factors levels means (null hypothesis), a test statistic or *F* ratio (F_0) was firstly computed. Next, this F_0 was compared to the corresponding upper-tail percentage point of an *F* distribution ($F_{critical}$). Finally, when $F_0 > F_{critical}$, the null hypothesis was rejected, and it was concluded that differences in the factors levels means do exist indeed. For further details about the analysis of variance carried out in this work, the interested reader my refer to the book by Montgomery [41].

It is also worth mentioning that, for the analyses of variance involving the product particles size, the percentages of mass passing through the 200 mesh (75 μm opening) were utilized. This was done because the size associated with the 80-passing mass criterion (P_{80}, mesh size through which 80% of the mineral passes) is smaller than the one corresponding to the finest mesh used in this work (200 mesh). If P_{80} had been used in this study, it would have been necessary to use a new mesh distribution and to perform the granulometry on a wet basis, which adds complexity to the sieving process. In the continuous milling tests, in addition, for the analysis of variance requiring representative values of the parameters accounted for, the average of the last three values of the percentages of mass passing through the 200 mesh (minutes 40, 50, and 60) was utilized. Finally, for the analysis of variance related to the energy consumption, the energy consumed per replicate, i.e., the area under the consumed power curve as a function of time, was employed. This was done for both batch and continuous ball milling tests.

4.2. *Results and discussions*

The main results obtained from the energy consumption-based characterization of the chalcopyrite milling tests carried out are discussed in this section. For the sake of brevity, the results obtained in both batch and continuous flow processing modes are presented and discussed together. In addition, from the two replicates performed for each milling test, the one that most clearly defines the trends in the results is discussed here.

4.2.1. *Product particles size*

The mass passing percentages of the first replicate of the ball mill tests, carried out in both batch and continuous processing modes, are shown in Fig. 9. More specifically, the vertical bars characterizing both the meshes and the conditions (slurry solids and mill speed at batch mode, grinding time in continuous mode) accounted for indicate the mass of mineral that remained on the sieve after the corresponding sieving. For the specific case of the batch milling tests (Fig. 9, left), the highest values in the bar graph, identified as Mesh −200, indicate the mineral discarded in the initial 200 mesh sieving of the wet mineral-slurry. From Fig. 9 (left), it is observed that most of the processed mineral passes through all meshes. However, the same does not occur in the case of the continuous milling tests (Fig. 9, right). Notice that Fig. 9 (right) results correspond to a 66% solids content.

In addition, Fig. 10 highlights the percentage of mass passing through the 200 mesh characterizing the second replicate of the milling tests carried out here. The left side of this figure corresponds to the milling tests performed in batch, whereas the right one to those carried out in continuous processing mode. Regarding the batch milling tests (Fig. 10, left), it is observed that, with the increase in the mill speed, the referred mass passing percentage increases as well. Consequently, the higher the mill speed, the smaller the average size of the product mineral particles. From Fig. 10 (left), it is also noticed that the 200 mesh mass passing decreases with the decrease in the solids concentration in the mineral-slurry. Notice also that the differences between the mass passing percentages at different solids contents decrease with the increase in the mill speed. This las outcome can be partially attributed to the increase in the number of collisions that occur inside the ball mill, regardless of whether they occur between grinding media, water, or ore.

The percentage of mass passing through the 200 mesh in the second replicate of the grinding tests performed in continuous mode, as a function of grinding time, is shown in Fig. 10 (right). As observed from this figure, the product particles initially present similar sizes for the three solids concentrations, 66, 70, and 75%, studied here. With the increase in the grinding time, however, the product particles size decreases, so the percentage mass passing through the 200 mesh tends to decrease as well. In particular, according to the results shown in Fig. 10 (right), at minute 60, the average particle size for a 66% slurry solids is larger than that characterizing a 75% one. These results can be associated with the fact that, as the chalcopyrite ore is more diluted in water (lower solids content), there is a larger recirculation of solid particles to the mill feed. This higher circulation load makes grinding more difficult, so the mill discharge becomes coarser [42]. It is worth noticing here that the product particles size, observed when analyzing the samples extracted at the classifier discharge, has a time lag response. This occurs because of the inherent characteristics of the classifier employed in this work, in which fine particles float for some time until they are discharged from the system by overflow.

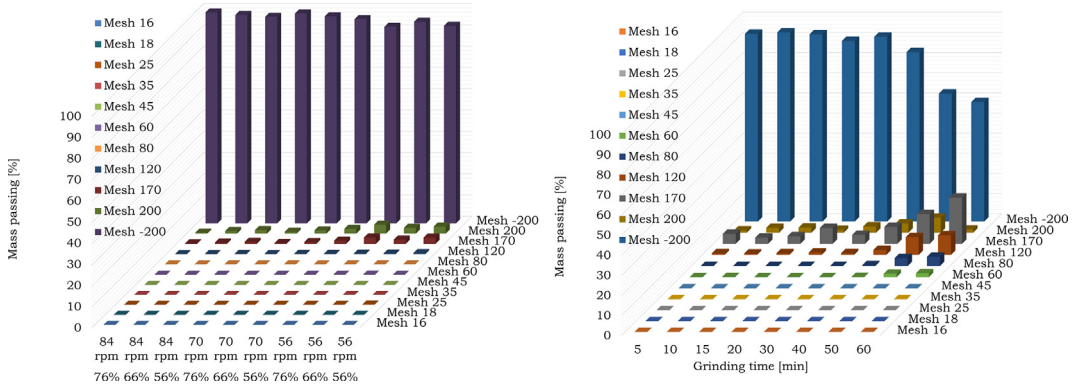

Fig. 9 – Percentages of mass passing of the ball milling tests (replicate 1) in batch (left) and continuous (right, 66% solids content) processing modes.

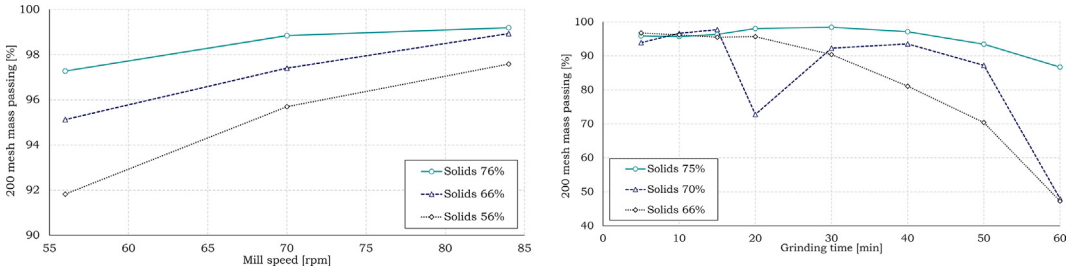

Fig. 10 – Percentage of mass passing through the 200 mesh characterizing the ball milling tests (replicate 2) in batch (left) and continuous (right) processing modes.

In addition, as emphasized by the results shown in Fig. 10, the size of the product obtained from the grinding processes varies with the concentration of solids in the slurry, which is controlled here through the water mass flow rate fed to the system. This is more evident in the continuous ball milling tests results, which indicate that the lower the slurry solids content, the smaller the amount of mass passing through the 200 mesh. This means that, as the amount of feed water increases, the solids concentration decreases, and less fine product is produced (product is coarser). In the continuous ball milling tests, specifically, by increasing the feed water to decrease the slurry solids from 75 to 66%, the percentage of product passing through the 200 mesh is reduced about 25%. Finally, as indicated above, the results shown in Fig. 9 and Fig. 10 correspond to specific test replicates only. When comparing these results to those ones coming from the test replicates not shown here, some discrepancies between the tests' replicates related results are observed. More specifically, in relative terms, the referred discrepancies in the batch tests are relatively small (average $< 0.5\%$), whereas in the continuous ones they are larger (average $\sim 6\%$).

4.2.2. *Energy consumption*

Regarding the energy consumed during the ball milling tests carried out, Fig. 11 shows the temporal evolution of the mill power draft characterizing both batch and continuous experimental tests. Concerning the batch milling tests, specifically, Fig. 11 (left) shows that, when using different mills speeds, relatively large differences in energy consumption appear. Indeed, in the tests first replicate, for mill speeds of 84, 70, and 56 rpm, the power draw of the batch mill is about 270, 220, and 180 W, respectively. It is worth noticing here that the mechanical power supplied to the mill, which is directly proportional to the electrical energy consumed during the grinding processes, is equal to the mill speed times the torque exerted by the motor. In the batch milling tests performed, the motor torque is relatively constant. Therefore, as observed from Fig. 11 (left), the energy consumed during the milling tests is directly proportional to the mill speed, i.e., the higher the mill speed, the higher the mill power draft. From this figure, it is also noticed that the power draft fluctuations increase with the increase in the mill speed. This outcome can be associated with the erratic movement of the steel balls inside the batch mill that is caused by the increase in the mill speed. In this regard, previous works [39] emphasize that, to obtain an efficient grinding, an orderly and cascade-type ball movement needs to take place inside the mill. Finally, according to the results shown in Fig. 11 (left) and when compared to the mill speed, the solids content in the mineral slurry has a smaller influence on the energy consumed in the grinding processes. Notice that, in both replicates of the batch experiments carried out and regardless of the mill speed, those tests involving a 56% solids content featured the lowest energy consumption. This result can be attributed to both the lower concentration of mineral in the slurry, and the lower probability of collisions between grinding media (balls) and mineral. In other words, the energy consumed in these situations is mainly associated with the collision of grinding media with water and not with the chalcopyrite ore being ground [39].

The temporal evolution of the mill power draft characterizing the continuous milling tests is shown, in turn, in Fig. 11 (right). Observing the details of the energy consumption related curves shown in this figure, it can be noticed that, until

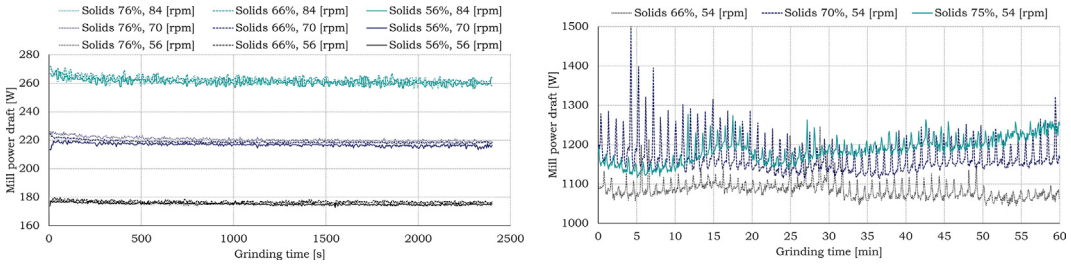

Fig. 11 – Temporal evolution of the mill power draft characterizing the ball milling tests (replicate 1) in batch (left) and continuous (right) processing modes.

around minute 15, power drafts at 70 and 75% solids content are similar. From this point and onwards, the higher energy consumption associated with the 75% slurry solids becomes more evident. Similarly, the relatively large power draft oscillations, which initially are of up to 300 W, decrease to less than 150 W. From Fig. 11 (right), it can be also noticed that, for the three slurry solids contents studied in this work, the energy consumption varies slightly only, and that these differences seem to become larger with increasing grinding time. In particular, the higher the slurry solids content, the higher the energy consumption. The increase in energy consumption with the increase in the slurry solids can be associated with the increase in the slurry viscosity (Fig. 7, right), which results from the increase in the number of particle–particle interactions. Mechanically, this outcome implies that the torque to be overcome by the mill motor is higher. As noticed from Fig. 11 (right), however, the associated differences in power consumption are not so significant. This occurs because the ore feed rate and the mill steel ball charge are the same for the three solids concentrations studied here. In the continuous milling tests performed, indeed, the feed water to the system (pilot plant) is the only parameter (control factor) that varies. It is worth noticing here that the ball mill loading, i.e., grinding media (steel balls) and product (chalcopyrite ore), is the system parameter that influences the most the mill torque.

The total grinding energy associated with all batch and continuous ball milling tests (replicates 1 and 2) carried out in this work are summarized in Table 6. The grinding energy values (in Wh) shown in this table come from integrating the area under the curves of mill power draft versus time characterizing the milling tests. As such, they represent the total energy consumed per test replicate. More specifically, Table 6 last column highlights the energy relative discrepancies between the tests' replicates. As noticed from these results, the referred discrepancies in the batch tests are relatively small (average < 0.3%), whereas in the continuous ones these discrepancies are larger (average < 5%).

In addition, in accordance with the results shown in Fig. 11 (left), the grinding energy ones characterizing the batch milling tests (Table 6) indicate that mill speed significantly affects the associated energy consumption. The reasons for this outcome were emphasized above. However, the same does not occur in the case of the slurry solids content. Indeed, Table 6 results highlight that, for a given mill speed and regardless of the processing mode (batch or continuous), the grinding energy values associated with different slurry solids contents vary slightly only. Even so, the energy consumption in the continuous milling tests tends to slightly increase with the increase in the slurry solids concentration. In other words, energy consumption tends to decrease with increasing mill feed water.

4.2.2.1. *Comparison with previous works*. To compare the results obtained in this work with others available in literature, the specific grinding energy (in kWh/ton) associated with the ball milling tests carried out has been estimated. The referred specific grinding energy has been computed by dividing the total grinding energy (energy consumed per test replicate) by the mass of product passing through the 200 mesh. Accordingly, Fig. 12 shows the product size (percentage of mass passing through the 200 mesh) versus the specific grinding energy for specific replicates of the batch and continuous milling tests carried out. Notice that, to easily compare these results with P_{80} related ones available in previous works, Fig. 12 vertical axis values are shown in reverse order. This has been done because the percentage of mass passing through a 200 mesh and P_{80} are inversely proportional, i.e., when the former increases, the latter decreases, and vice versa.

Regarding the results obtained from the batch mode milling tests, specifically, Fig. 12 (left) shows that the lowest specific energy consumption comes from the lowest mill speed (56 rpm). Furthermore, for a given mill speed, the lowest specific energy consumption is originated from the highest solids concentration (76%). Comparing these results with other similar ones available in literature [43], it is observed that the trends are the same. This occurs even though the comparison between these results cannot be directly made, since there the P_{80} parameter is employed. In particular, from Fig. 12 (left), for the same percentage of mass passing the 200 mesh (or the same P_{80} in [43]), both (i) as the concentration of solids in the slurry increases, the specific grinding energy decreases, and (ii) the specific energy consumption increases with the increase in the mill speed.

Like in the case of the batch milling tests, the specific grinding energy results associated with the continuous mode milling tests (pilot plant) have been estimated and compared

Table 6 – Total grinding energy characterizing both batch and continuous ball milling tests.

Processing mode	Mill speed [rpm]	Slurry solids [%]	Grinding energy [Wh] Replicate 1	Grinding energy [Wh] Replicate 2	Replicates relative differences [%]
Batch	56	56	116.8	115.7	0.48
	56	66	117.8	116.0	0.78
	56	76	117.3	116.6	0.28
	70	56	144.6	145.7	0.39
	70	66	145.9	145.9	0.01
	70	76	147.0	146.1	0.32
	84	56	173.9	174.1	0.05
	84	66	174.9	174.3	0.19
	84	76	174.6	174.2	0.12
Continuous	54	66	1082.0	1092.0	0.90
	54	70	1162.0	1082.0	−6.88
	54	75	1184.0	1115.0	−5.78

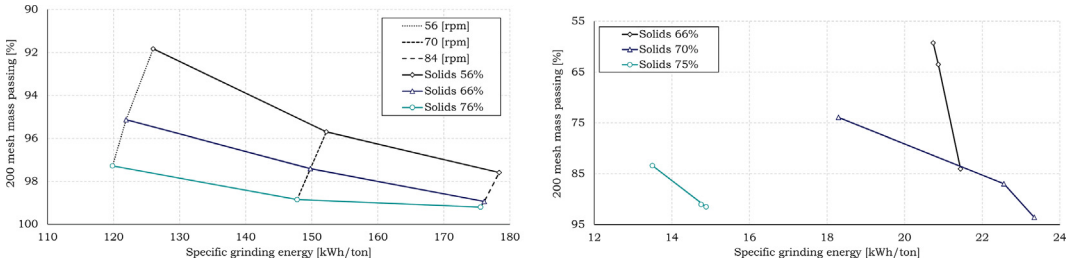

Fig. 12 – Relationship between product size (percentage of mass passing through the 200 mesh) and specific grinding energy. Batch (left, replicate 2) and continuous (right, replicate 1) ball milling tests.

with previous ones [43]. It is worth noticing that, for these specific comparisons, the last three energy consumption related values from each replicate, which show more clearly the trends and differences between each studied condition, have been accounted for. As such, for each slurry solids concentration, the three points shown in Fig. 12 (right) correspond to the specific grinding energy characterizing grinding times 40, 50, and 60 min. Figure 12 (right) shows that, for the same percentage of mass passing the 200 mesh, the higher the slurry solids content, the lower the specific grinding energy. This behavior agrees with that observed in the batch milling cases (Fig. 12, left). Mill power drafts as a function of mineral-slurry density, expressed in terms of solids concentration, are also discussed in literature. In accordance with previous works [40], thus, results (not shown here for the sake of brevity) obtained from the continuous mode milling tests carried out show that mill power draft increases with the increase in solids concentration. Therefore, the results obtained here, in both batch and continuous processing modes, agree with others available in previous studies carried out using other milling systems.

4.2.3. *Analysis of variance results*

As mentioned before, to determine whether the levels of the studied factors (mill speed and slurry solids) affect indeed the parameters of interest (product particles size and energy consumption), an analysis of variance based statistical analysis was also performed. The referred analysis of variance was carried out following the methodology highlighted in Section 4.1.5. Accordingly, regarding the first response variable, i.e., product particles size, the analysis of variance performed led to F_0 values higher than their corresponding $F_{critical}$ ones. This means that, statistically, the null hypothesis (hypothesis of no differences in factors levels means) can be rejected and the alternative one accepted. In other words, both mill speed and slurry solids contents have a statistical significance in the product particles size (percentage of mass passing through the 200 mesh). This occurred for both batch and continuous mode tests, although in the continuous ones, the slurry solids content was the only parameter varied. Notice that this analysis of variance related outcome agrees with Fig. 10 results discussed above.

Regarding the second response variable, i.e., energy consumption, in turn, the analysis of variance carried out indicates that the only factor having a statistical significance in the energy consumption response variable is the mill speed, being this significance relatively high. When using the slurry solids content as a factor, indeed, in both batch and continuous milling tests, the energy consumption related analysis of variance led to F_0 values lower than their corresponding $F_{critical}$ ones. This means that, it statistical terms, the measured values of energy consumption are not sufficient to reject the null hypothesis. These analysis of variance results are in accordance with those shown in Table 6, where the grinding energy characterizing milling tests featuring different slurry solids contents vary slightly only. Although the slurry solids content has no statistical significance in the associated response, energy consumption in the continuous milling tests seems to slightly increase with the increase in the slurry solids content. To be fully conclusive, however, these lab-scale mill results need to be complemented with others obtained from large-scale ball mills used in actual concentrator plants.

5. Conclusions

A detailed characterization of chalcopyrite ball mill grinding processes, in both batch and continuous flow processing modes, has been carried out in this work. The referred characterization involved different mineralogical, rheological and energy consumption-related aspects. Firstly, chalcopyrite (copper) ore samples were mineralogically characterized using both X-ray diffraction and optical microscopy techniques, which allowed identifying the presence of 5% chalcopyrite in the ore samples analyzed. An initial study of batch grinding processes focused on assessing particle size distribution, grindability characteristics, and work index was next performed. The chalcopyrite granulometric analysis performed using the standard meshes method allowed determining the referred particle size distribution. By extrapolating the obtained results, the F_{80} characterizing the chalcopyrite samples accounted for was determined. As this parameter is equal to 1386 μm here, 80% of the particles present in the chalcopyrite head ore have a diameter smaller than 1386 μm. The grindability tests carried out using a standard Bond ball mill allowed, in turn, determining the product particle size distribution of the processed ore as a function of both grinding time and work input. Results from such tests were used to compute the Bond ball mill work index characterizing the chalcopyrite ore analyzed here. The calculated work index

is equal to 15.3 kWh/ton, which corresponds to a mineral with presence of chalcopyrite.

Secondly, a rheological study of actual and lab ground chalcopyrite mineral-slurries was performed. More specifically, two sets of mineral-slurry samples were analyzed. The first set involved actual mineral-slurry samples extracted from a ball mill discharge section of a copper concentrator plant. The second set included, in turn, four additional slurries featuring different solids concentrations (50, 60, 66, and 70%), which were artificially created in a lab using the chalcopyrite head ore studied in this work. The main results obtained from the referred rheological characterization indicate that, at the slurry solids contents analyzed, all actual and lab ground mineral-slurries exhibit a shear thinning rheological behavior. However, the actual mineral-slurry features viscosity levels slightly higher than those associated with the corresponding lab created one. The results also show that, because of the larger number of particle interactions, the slurries apparent viscosity increases with the increase in their solids concentration. Using the experimental data obtained here, material coefficients associated with the non-Newtonian Carreau-Yasuda model were determined as well. These coefficients will be useful in the numerical modeling of transport and grinding processes involving the mineral-slurries accounted for here. In addition, when compared to previous results, the experimental rheological ones obtained here present reasonably agreement, which supports the findings discussed in this work.

Finally, an energy consumption-based characterization of several chalcopyrite ball mill grinding processes, carried out in both batch and continuous flow processing modes, was performed. The referred grinding studies sought to determine the influence of both mill speed and slurry solids content on the product particles size and the associated energy consumption. This was done because the mill speed directly affects the mechanical power required to drive the mill. In turn, the slurry solids content increases or decreases particle–particle collisions, which varies the slurry viscosity and translates into the torque required from the mill motor. In all milling tests, the concentration of solids in the slurry was varied by regulating the mill feed water. The results obtained here allowed identifying that energy consumption is more significantly affected by the mill speed than the slurry solids content. It was also found that, for the same percentage of mass passing the 200 mesh, the specific grinding energy decreases with both the increase in the slurry solids concentration, and the decrease in the mill speed. The energy consumption related results obtained in this work are consistent with findings made in previous studies. In addition, as highlighted by the rheological results, the slurry viscosity increases with the increase in its solids concentration, limiting the rotational movement of the mill drum, and leading to an increase in energy consumption. The opposite behavior however, of lower viscosity with higher shear rate, has not been confirmed through the results obtained from the batch and continuous milling tests performed here. This is because the decrease in energy consumption due to the lower apparent viscosity, caused by the higher shear rate, is negligible compared to the increase in energy consumption due to other factors such as mill speed.

Declaration of Competing Interest

The authors declare that they have no known competing financial interests or personal relationships that could have appeared to influence the work reported in this paper.

Acknowledgments

This work has been funded by CONCYTEC-FONDECYT (PROCIENCIA) (Peru) within framework E041-01, Contract No. 155-2018-FONDECYT-BM-IADT-AV. The authors would like to thank all people that contributed to the development of this work, especially to Mr. J. Leyton, Mr. A. Pando, Mr. J. Lopez, and Mr. M. Shishido.

REFERENCES

[1] Gupta A, Yan DS. Mineral processing design and operations, an introduction. 2nd ed. New York, US: Elsevier; 2016.
[2] Fuerstenau DW, Abouzeid A-ZM. The energy efficiency of ball milling in comminution. Int J Miner Process 2002;67:161–85.
[3] Fueyo CL. Equipos de trituración, molienda y clasificación: tecnología, diseño y aplicación. Madrid, Spain: Rocas y Minerales; 2002.
[4] Napier-Munn T. Is progress in energy-efficient comminution doomed? Miner Eng 2015;73:1–6.
[5] Levesque M, Millar D, Paraszczak J. Energy and mining–the home truths. J Clean Prod 2014;84:233–55.
[6] Wills BA, Finch JA. Chapter 5 - comminution. In: Wills BA, Finch JA, editors. Wills' mineral processing technology. 8th ed. 2016.
[7] Sabah E, Özdemir O, Koltka S. Effect of ball mill grinding parameters of hydrated lime fine grinding on consumed energy. Adv Powder Technol 2013;24:647–52.
[8] Ouattara S, Frances C. Grinding of calcite suspensions in a stirred media mill: effect of operational parameters on the product quality and the specific energy. Powder Technol 2014;255:89–97.
[9] Taylor L, Skuse D, Blackburn S, Greenwood R. Stirred media mills in the mining industry: material grindability, energy-size relationships, and operating conditions. Powder Technol 2020;369:1–16.
[10] Mende S, Stenger F, Peukert W, Schwedes J. Mechanical production and stabilization of submicron particles in stirred media mills. Powder Technol 2003;132:64–73.
[11] Stenger F, Mende S, Schwedes J, Peukert W. The influence of suspensions properties on the grinding behaviour of alumina particles in the sub-micron size range in stirred media mills. Power Technology 2005;156:103–10.
[12] Faitli J, Bohács K, Mucsi G. Online rheological monitoring of stirred media milling. Powder Technol 2017;308:20–9.
[13] Shi F, Morrison R, Cervellin A, Burns F, Musa F. Comparison of energy efficiency between ball mills and stirred mills in coarse grinding. Miner Eng 2009;22:673–80.
[14] Altun D, Gerold C, Benzer H, Altun O, Aydogan N. Copper ore grinding in a mobile vertical roller mill pilot plant. Int J Miner Process 2015;136:32–6.
[15] Altun D, Benzer H, Aydogan N, Gerold C. Operational parameters affecting the vertical roller mill performance. Miner Eng 2017:67–71. 103–104.

[16] Shi F, Xie W. A specific energy-based ball mill model: from batch grinding to continuous operation. Miner Eng 2016;86:66–74.
[17] Garcia F, Le Bolay N, Frances C. Changes of surface and volume properties of calcite during a batch wet grinding process. Chem Eng J 2002;85:177–87.
[18] Italica Societa Mineraria del Peru. http://www.italicamineraria.com/.
[19] BIZALab SAC. https://www.bizalab.com.pe/.
[20] Quiroz I. Ingeniería metalúrgica: operaciones unitarias en procesamiento de minerales. 1986 [Lima].
[21] Bond FC. Crushing and grinding calculations. Br Chem Eng 1961;6:378–85.
[22] Mular AL, Halbe DN, Barratt DJ. Mineral processing plant design, practice, and control. Proceedings of the Society for Mining, Metallurgy, and Exploration; 2002 [SME)].
[23] Abulnaga BE. Slurry systems handbook. McGraw-Hill; 2002.
[24] Michaelides E, Crowe CT, Schwarzkopf JD. Multiphase flow handbook. CRC Press; 2016.
[25] TA instruments. https://www.tainstruments.com/.
[26] Chun J, Poloski AP, Hansen EK. Stabilization and control of rheological properties of Fe_2O_3/$Al(OH)_3$-rich colloidal slurries under high ionic strength and pH. J Colloid Interface Sci 2010;348:280–8.
[27] Zhang M, Peng Y. Effect of clay minerals on pulp rheology and the flotation of copper and gold minerals. Miner Eng 2015;70:8–13.
[28] Blakey BC, James DF. Characterizing the rheology of laterite slurries. Int J Miner Process 2003;70:23–39.
[29] Bhattacharya IN, Panda D, Bandopadhyay P. Rheological behaviour of nickel laterite suspensions. Int J Miner Process 1998;53:251–63.
[30] Phillips RJ, Armstrong RC, Brown RA, Graham AL, Abbott JR. A constitutive equation for concentrated suspensions that accounts for shear-induced particle migration. Phys Fluid Fluid Dynam 1992;4:30–40.
[31] Siqueira IR, Carvalho MS. Particle migration in planar die-swell flows. J Fluid Mech 2017;825:49–68.
[32] Mangesana N, Chikuku RS, Mainza AN, Govender I, van der Westhuizen AP, Narashima M. The effect of particle sizes and solids concentration on the rheology of silica sand based suspensions. J S Afr Inst Min Metall 2008;108:237–43.
[33] Barnes HA, Hutton JF, Walters K. An introduction to rheology. Elsevier; 1989.
[34] Chossat P, Looss G. The Couette–taylor problem. New York: Springer-Verlag; 1994.
[35] Bird RB, Stewart WE, Lightfoot EN. Transport phenomena. New York: John Wiley & Sons; 2002.
[36] Sun L, Zhang X, Tan W, Zhu M, Liu R, Li C. Rheology of pyrite slurry and its dispersant for the biooxidation process. Hydrometallurgy 2010;104:178–85.
[37] Singh J, Kumar S, Singh JP, Kumar P, Mohapatra SK. CFD modeling of erosion wear in pipe bend for the flow of bottom ash suspension. Part Sci Technol 2018;37:275–85.
[38] Weiss NL. SME mineral processing handbook. New York, US: Society of Mining Engineering, American Institute of Mining, Metallurgical and Petroleum Engineers, Inc.; 1985.
[39] Austin LG, Concha F. Diseño y simulación de circuitos de molienda y clasificación, CYTED, Programa Iberoamericano de ciencia y tecnología para el desarrollo. 1994.
[40] Gao M-W, Forssberg KSE, Weller KR. Power Predictions for a pilot scale stirred ball mill. Int J Miner Process 1996;44–45:641–52.
[41] Montgomery DC. Design and analysis of experiments. 8th ed. John Wiley & Sons; 2013.
[42] Yianatos JB, Lisboa MA, Baeza DR. Grinding capacity enhancement by solid concentration control of hydrocyclone underflow. Miner Eng 2002;15:317–23.
[43] Jankovic A. Variables affecting the fine grinding of minerals using stirred mills. Miner Eng 2003;16:337–45.